Carderock Division, Naval Surface Warfare Center
West Bethesda, Maryland 20817-5700

NSWCCD-50-TR-2003/014 February 2003

Hydromechanics Directorate
Research and Development Report

Velocity Measurements Inside the Pump of the Gulf Coast Waterjet Tow Tank Model 5600

by

Christopher J. Chesnakas

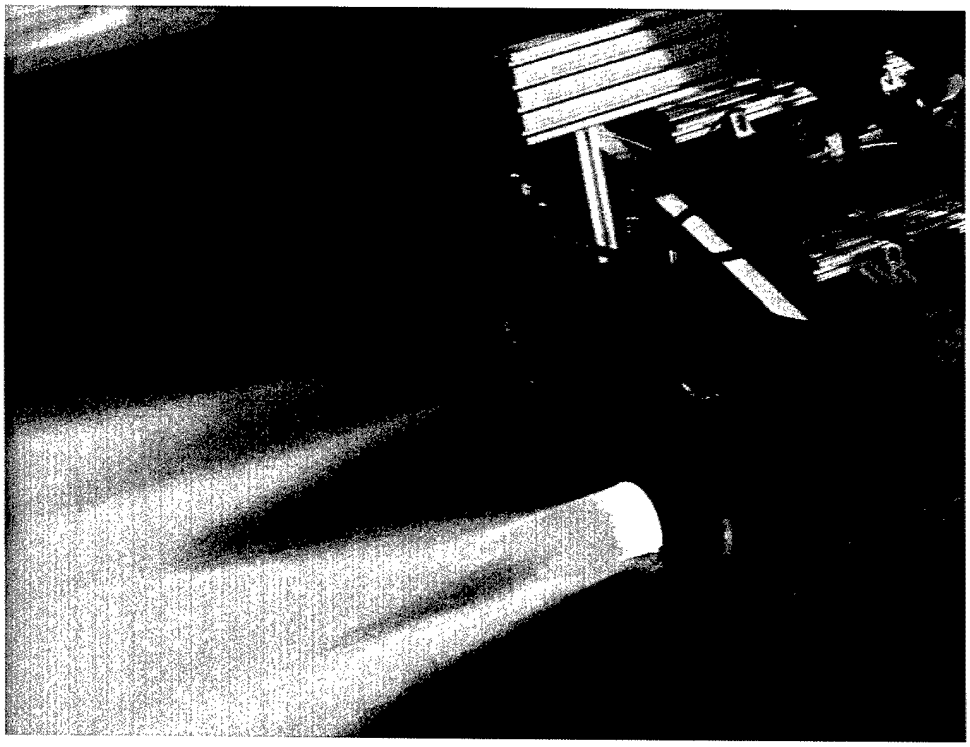

REPORT DOCUMENTATION PAGE

Form Approved
OMB No. 0704-0188

1. REPORT DATE *(DD-MM-YYYY)*	2. REPORT TYPE	3. DATES COVERED *(From - To)*
February 2003	Technical	April - June 2002

4. TITLE AND SUBTITLE
Velocity Measurements Inside the Pump of the Gulf Coast Waterjet Tow Tank Model 5600

5a. CONTRACT NUMBER

5b. GRANT NUMBER

5c. PROGRAM ELEMENT NUMBER
0602123N

6. AUTHOR(S)
Christopher J. Chesnakas

5d. PROJECT NUMBER

5e. TASK NUMBER

5f. WORK UNIT NUMBER
02-1-0100-201

7. PERFORMING ORGANIZATION NAME(S) AND ADDRESS(ES) AND ADDRESS(ES)

Naval Surface Warfare Center
Carderock Division
9500 Macarthur Boulevard
West Bethesda, MD 20817-5700

8. PERFORMING ORGANIZATION REPORT NUMBER

NSWCCD-50-TR-2003/014

9. SPONSORING / MONITORING AGENCY NAME(S) AND ADDRESS(ES)
Office of Naval Research
Ballston Center Tower One
800 N. Quincy Street
Arlington, VA 22217

10. SPONSOR/MONITOR'S ACRONYM(S)

11. SPONSOR/MONITOR'S REPORT NUMBER(S)

12. DISTRIBUTION / AVAILABILITY STATEMENT
Approved for public release. Distribution unlimited.

13. SUPPLEMENTARY NOTES

14. ABSTRACT

An internal, three-component LDV system was used to measure the flow ahead of the rotor and inside the nozzle of a waterjet installed in a model of the R/V Athena hull as part of a program to develop performance prediction methods for marine waterjet propulsion systems. These tests revealed the flow structure within the pump, and allowed the calculation of terms required for an analysis of the pump performance. The pump was tested at three underway speeds at the self-propulsion point and at two bollard conditions.

15. SUBJECT TERMS
Waterjet, LDV

16. SECURITY CLASSIFICATION OF:			17. LIMITATION OF ABSTRACT	18. NUMBER OF PAGES	19a. NAME OF RESPONSIBLE PERSON
a. REPORT	b. ABSTRACT	c. THIS PAGE			Christopher Chesnakas
UNCLASSIFIED	UNCLASSIFIED	UNCLASSIFIED	Unlimited	35	19b. TELEPHONE NUMBER *(include area code)* (301) 227-5833

(THIS PAGE INTENTIONALLY LEFT BLANK)

CONTENTS

	Page
SYMBOLS	v
ABSTRACT	vi
ADMINISTRATIVE INFORMATION	1
INTRODUCTION	1
EXPERIMENTAL APPARATUS	1
Hull	1
Propulsors	1
Probes	2
Traverse	2
Windows	3
Seeding	3
Signal Processing	3
PROCEDURE	3
Test Conditions	3
Data Acquisition	4
Data Reduction	5
Velocity Components	5
Integrated Flux Coefficients	6
EXPERIMENTAL RESULTS	6
Velocity Planes	6
Integrated Flux Coefficients	8
UNCERTAINTY ANALYSIS	9
Elemental Uncertainties	9
Calculated Uncertainties	9
CONCLUSIONS	11
ACKNOWLEDGEMENTS	12

FIGURES

1. Model 5600 hull, side view.	13
2. R/V Athena.	13
3. Model 5600 propulsor, cutaway view.	13
4. Model 5600 hull and pump cutaway.	14

5. Probe assembly. 14
6. Shadowed regions of flow, Station 3. 14
7. Probe assembly on model at station 6. 15
8. Probe assembly on model at station 3. 15
9. Probes in water tank on model at station 6. 16
10. Waterjet operation at bollard. 16
11. Waterjet operation underway. 17
12. Axial velocity, station 3, 25 kt. full scale. 18
13. Axial velocity fluctuation, station 3, 25 kt. full scale. 18
14. Axial velocity, station 6, 25 kt. full scale. 19
15. Axial velocity, station 6, 16.67 kt. full scale. 19
16. Axial velocity, station 6, 8.33 kt. full scale. 20
17. Axial velocity, station 6, 1400 rpm bollard. 20
18. Axial velocity, station 6, 1000 rpm bollard. 21
19. Velocity fluctuations, station 6, 25 kt. full scale. 22
20. Velocity fluctuations, station 6, 16.67 kt. full scale. 22
21. Velocity fluctuations, station 6, 8.33 kt. full scale. 23
22. Velocity fluctuations, station 6, 1400 rpm bollard. 23
23. Velocity fluctuations, station 6, 1000 rpm bollard. 24
24. Measured waterjet flow rate. 24
25. Bias uncertainty in axial velocity, station 3, 25 kt full scale. 25
26. Total uncertainty in axial velocity, station 3, 25 kt full scale. 25
27. Bias uncertainty in axial velocity, station 6, 25 kt full scale. 26
28. Total uncertainty in axial velocity, station 6, 25 kt full scale. 26
29. Total uncertainty in horizontal velocity, station 6, 25 kt full scale. 27
30. Total uncertainty in vertical velocity, station 6, 25 kt full scale. 27
31. Total uncertainty in axial velocity, station 6, 1400 rpm bollard. 28

TABLES

1. Test conditions. 4
2. Hull and rotor speeds. 7
3. Integrated Flux Coefficients, underway. 8
4. Integrated Flux Coefficients, bollard. 9
5. Elemental uncertainties. 9

SYMBOLS

B	Bias uncertainty
D_R	Diameter of the rotor, 4.82 inches
Fn	Froude number, $U_\infty / \sqrt{gL}$, where g is acceleration due to gravity
L	Length of hull at waterline, 216.0 inches
P	Precision (random) uncertainty
Q	Volume flow rate
q	Root-mean-square (RMS) fluctuation of velocity, TKE = $\rho q^2/2$, normalized by U_∞
u	Root-mean-square (RMS) fluctuation of axial velocity component
$U(U_i)$	Total uncertainty in velocity component U_i, normalized by U_∞
U_r	Velocity radially outward from shaft axis, normalized by U_∞
U_t	Velocity tangential to shaft axis, normalized by U_∞
U_x	Velocity in direction of model axis, normalized by U_∞ (+ downstream)
U_y	Velocity in horizontal direction, perpendicular to model axis, normalized by U_∞ (+ starboard)
U_z	Velocity in vertical direction, normalized by U_∞ (+ up)
U_∞	Model speed
x	Coordinate along hull axis, from bow waterline, normalized by L
y	Coordinate in transverse direction, from centerline, normalized by L (+ starboard)
z	Coordinate vertical direction, from waterline, normalized by L (+ up)
β_E	Energy non-uniformity coefficient, see Equation 6
β_M	Momentum non-uniformity coefficient, see Equation 5
θ_3	Angle between measured velocity component 3 and z axis

(THIS PAGE INTENTIONALLY LEFT BLANK)

ABSTRACT

An internal, three-component LDV system was used to measure the flow ahead of the rotor and inside the nozzle of a waterjet installed in a model of the R/V Athena hull as part of a program to develop performance prediction methods for marine waterjet propulsion systems. These tests revealed the flow structure within the pump, and allowed the calculation of terms required for an analysis of the pump performance. The pump was tested at three underway speeds at the self-propulsion point and at two bollard conditions.

ADMINISTRATIVE INFORMATION

This work was performed between April and May of 2002 at the Naval Surface Warfare Center, Carderock Division under Work Unit number 02-1-0100-201. Funding for the project came from the NSWCCD Internal Applied Research (IAR) program funded by the Office of Naval Research under program element 0602123N.

INTRODUCTION

This program was intended to provide validation data to support performance prediction methods for marine waterjet propulsion systems that will account for interactions between the inlet and hull, and between the hull and jet flow. The project includes both computational and experimental investigations of waterjet/hull interactions. As a part of this program, model tests of a scale hull and with waterjets were conducted in the David Taylor Model Basin at the Naval Surface Warfare Center, Carderock Division (NSWCCD). This report documents the measurements of velocity within the waterjets using an internal Laser Doppler Velocimetry (LDV) system.

EXPERIMENTAL APPARATUS

Hull

The hull used in the test, Model 5600, is shown in Fig. 1. Model 5600 is a 216-inch long version of the RV Athena, shown in Fig. 2, an NSWCCD research vessel of overall length 165 ft and beam of 24ft. The model scale ratio is 8.556. The hull has been modified from the actual ship by the elimination of the two external shafts and propellers, and the addition of two waterjet propulsors. The model has no rudders.

Propulsors

The hull was fitted with two waterjets designed by a joint team of NSWCCD and Band, Lavis and Associates, as shown in Figs. 3 and 4. The intakes for the pumps were elliptical openings on the bottom

of the hull, and the outlets of the waterjets were circular nozzles on the stern with the centerline at the resting waterline. The axis of each pump was horizontal, and parallel to the ship axis. The pumps each had a shaft driven rotor with 7 blades followed by an 11 blade stator. The pump casing is cylindrical throughout the stage. The pump nozzle contracted from 4.85 inches at the stator exit to 3.33 inches at the discharge.

Probes

Two TSI Model 9812 25mm fiber-optic probes were used to measure the flow inside the pump. The two probes were mounted together as shown in Fig. 5. The first probe was mounted vertically, and the second probe was mounted at 50° to the first probe, with the probe volume aligned to be coincident with control volume of the first probe. The probe arrangement, however, was different at each measurement station.

At the aft measurement station, station 6, the vertically mounted probe used the green (514.5nm) output of an argon-ion laser to measure velocity in the x-direction, and the blue (488nm) output to measure velocity in the y-direction. The second probe used the violet (476nm) output of the argon-ion laser to measure a component of velocity in the y-z plane at 50° to the y axis. In this way, three non-orthogonal velocity components were measured which could be transformed to any desired coordinate system.

At the forward measurement station, station 3, the vertically mounted probe used the blue (488nm) output to measure velocity in the x-direction, and the second probe used the violet (476nm) output of the argon-ion laser to measure velocity in the x-direction as well. This was done to minimize the regions of the flow which could not be measured. As shown in Fig. 6, the hub at station 3 blocks a considerable portion of the flow from being measured by each probe. The region blocked from being measured by both probes, however, is fairly small and was accounted for. With the arrangement used, the axial component of velocity is measured over most of station 3, instead of measuring all three components of velocity over a considerably smaller portion of station 3.

Traverse

The probe assembly was moved to the various measurement positions using a two-component, computer-controlled traverse. This traverse was bolted to the hull, and could be moved in both the vertical (z) and port-starboard (y) directions. The traverse is shown in place in Fig. 7.

Windows

In order to make measurements inside the pump, two 0.7-inch wide slots covering 220° of arc were cut into the starboard pump housing to allow optical access to the LDV probes. These slots were just ahead of the rotor at $x/L = 0.977$, and in the nozzle at $x/L = 1.008$. At these locations, the inside diameters of the pump were 4.860" and 3.384", respectively. In each slot was a with thin (0.030"), curved polycarbonate windows bonded to a stereo-lithography-produced resin frame that held the window flush with the inner surface. The windows prevented flow through the slots and ensured that the flow remained undisturbed. The arrangement of the windows is diagrammed in Fig. 4.

Surrounding each window was a tank which kept the probes immersed in water. In this way, as the probes traversed to various points in the flowfield, the optical path length remained equal, and the probe volumes remained aligned. These two tanks can be seen in Figs. 7 and 8. Fig. 9 shows how the probe assembly fit in the tank at station 6.

Seeding

The flow about the hull was seeded with 1500-grit silicon carbide powder, 1 to 2μm in size. The powder was mixed into a slurry with water and injected through nine 0.1-inch diameter taps in the hull at $x/L = 0.2$.

Signal Processing

Doppler signals were analyzed with a TSI Model IFA 655 Digital Burst Correlator. The processor performs a 256-sample, double-clipped, autocorrelation on each doppler burst, allowing the measurement of velocity even when the signal-to-noise ratio is low. In order to maximize data rate, the processors were operated in the random mode.

PROCEDURE

Test Conditions

All tests were performed on carriage 1 of the David Taylor Model Basin. The model was tested in the underway condition at three speeds corresponding to Froude Numbers of 0.2, 0.4, and 0.6. (8.33, 16.67 and 25 kt. full scale). At all speeds the model was free to pitch and heave and was allowed to obtain a steady trim at the desired speed. Waterjet speeds for the modeled self-propulsion point for these Froude Numbers were determined in previous experiments assuming the standard tow force augment to offset the excess viscous drag due to the Reynolds Number disparity.

Table 1. Test conditions.

Condition	Hull Speed (kt.) Model	Full	*Fn*	Rotor Speed rpm	Sinkage (in.)	Trim (deg.)
Underway	2.85	8.33	0.2	496	-0.04	0.09
Underway	5.70	16.67	0.4	999	-0.94	0.50
Underway	8.55	25	0.6	1467	-0.60	1.45
Bollard	0		0	1000	0	0
Bollard	0		0	1400	0	0

The measurements were also performed in a bollard condition (hull stationary in the water) to verify the waterjet flow rate calibration performed by conventional means. The model was backed part way into the drydock, with the stern of the model about 10 ft from the end wall of the drydock and the drydock door open. Data were then collected with the pumps running at 1000 rpm and 1400 rpm. Measurements were taken partially in the drydock so that seed particles could recirculate. The run conditions are listed in Table 1.

Measurements were made at station 3 (rotor inlet, x/L = 0.977) only at the 25 kt. underway condition (*Fn* = 0.6). Measurements were made at station 6 (nozzle, x/L = 1.008) at all test conditions.

The water surface was approximately at the centerline of the pump, so that when the pump was not operating, it was not completely flooded. To operate the pump, it first had to be primed. To do this, the pump speed was first set to approximately 1000 rpm, and the stern was pushed down in the water slightly. Once the pump was primed, the hull was allowed to return to its normal trim, the correct rpm was set, and the test could commence. At the bollard condition, the jet was about half way out of the water, as shown in Fig. 10. Underway, the jet was completely above the water surface, as shown in Fig. 11, due to the ventilation of the transom and resultant wave trough in the hull wake at the stern.

Data Acquisition

Before data were acquired, it was first necessary to obtain the position of the LDV measurement volume. This was done by using reference marks on the pump. At Station 6, a mark was placed on the lower surface of the pump wall. The probes were then moved to this mark with the hull submerged far enough to flood the nozzle. At station 3, the bottom pump wall was not easily visible with the pump flooded, so a different procedure was used. At station 3 a mark was placed on the outboard side of the pump window frame. This mark was used as a *y* reference, but made for a poor reference in the z direction (vertical) since the beams from the second probe were very distorted by the window at this mark without the pump flooded. To get the z reference, the probes were then traversed to the center plane of the pump, and moved vertically until the beams crossed at the top surface of the window.

At each axial location, a 19×19 grid of points in the flow was measured. This rectangular grid was transformed onto a circular grid to better fit the flow domain. During each carriage pass, the probe assembly was moved to different positions under computer control. Between 10 and 40 points could be obtained in each pass, depending on the model speed and data rate; lower towing speeds allowed longer runs, and thus more time for data collection.

At each measurement point in the flow, data were acquired for either 5 seconds or 80000 velocity realizations, whichever came first. Since the signal-to-noise ratio varied through the flow, the actual number measurements at each point in space varied. Data rate in the middle of the passage reached as high as 9000 samples per second on each channel, while near the wall data rate was between 1000 and 2000 samples per second. Data rate was generally nearly equal for the blue and green components, but the violet data rate was about 80% of that of the other two components. The number of data points from the violet channel was then lower than for the other two channels.

Data Reduction

Velocity Components

Three components of velocity, U_1, U_2, and U_3, were measured at station 6 with the present system, but the components were not aligned with the x, y, and z axes of the model, nor were they perpendicular. The measured velocities are transformed to the model coordinates by

$$U_x = U_1 \tag{1}$$

$$U_y = U_2 \tag{2}$$

$$U_z = \frac{U_3 - U_2 \cos\theta_3}{\sin\theta_3} \tag{3}$$

where θ_3 is the angle between the direction of the third component of velocity and the y axis, or 230°. The rms velocity, q, is calculated at station 6 by taking the square root of the sum of the variances in velocity of the three measured components.

At station 3, only the axial component of velocity was measured, so no transformations were needed. At locations where both probes measured the velocity, the reported velocity is the average of the two measurements. The rms of the axial velocity, u, is calculated at station 3 by taking:

- the square root of the variance in velocity if only one probe measured the velocity
- the square root of 0.5 times the sum of the variances in velocity if two probes measured the velocity.

Integrated Flux Coefficients

The velocity measurements can be integrated to obtain coefficients used in the calculation of the waterjet performance. To do this, the velocity measurements must first be interpolated to the wall. Grid points were added to the measurement set at the wall with axial velocity equal to 0.875 times the velocity at the nearest measured point to approximate the momentum of a turbulent boundary layer. The wall radial and tangential velocities were set to zero. For the points at station 3 in the hub shadow, velocities were linearly interpolated from nearby measurements at the same radius.

At each station, the flow rate, Q, was calculated by numerically integrating across the flow area

$$Q = \int U_x dA \tag{4}$$

Note that the integration area is perpendicular to the x-direction. The average velocity at each measurement plane, $\overline{U}$, is then simply Q/A.

The momentum and energy non-uniformity factors were calculated at each station by integrating

$$\beta_M = \frac{1}{A}\int \frac{U_x^2}{\overline{U}} dA \tag{5}$$

$$\beta_E = \frac{1}{A}\int \frac{U_x(U_x^2 + U_y^2 + U_z^2)}{\overline{U}^3} dA \tag{6}$$

Additionally, the energy non-uniformity factor could be divided into three parts, β_{Ex}, β_{Et}, and β_{Er}, to show the relative kinetic energy contributions from the axial, tangential, and radial (relative to the pump axis) velocity components. These terms are defined as

$$\beta_{Ex} = \frac{1}{A}\int \frac{U_x^3}{\overline{U}^3} dA \qquad \beta_{Et} = \frac{1}{A}\int \frac{U_x U_t^2}{\overline{U}^3} dA \qquad \beta_{Er} = \frac{1}{A}\int \frac{U_x U_r^2}{\overline{U}^3} dA \tag{7}$$

EXPERIMENTAL RESULTS

Velocity Planes

Measurements were obtained on a grid of 361 points at each plane as outlined in the *Procedure* section. At these planes, plots are shown with color contours of the velocity component in the direction of the model axis, U_x, and of the rms of the velocity fluctuations, q. Note that $\rho q^2/2$ is equal to the turbulent kinetic energy. For the plots at station 6, vectors of the in-plane velocities, looking upstream are plotted on top of the color contours. In all plots, distances are normalized by the ship length, L. In the

plots of the underway flowfield, velocities are normalized by the ship speed, U_∞, and in the plots of the bollard flowfield, velocities are normalized by the rotor tip speed, $\pi \cdot D_R \cdot$rpm/60. The contour levels and vector lengths on the plots at the bollard condition differ from those on the underway flow by about a factor of two. This is the approximate ratio of tip speed to hull speed for the underway conditions, as shown in Table 2, and should make the plots of the two conditions comparable.

Table 2. Hull and rotor speeds.

Hull Speed Full (kt.)	Model (ft/s)	Rotor Speed rpm	Tip Speed ft/s	Tip/Hull Speed
8.33	4.81	496	10.43	2.17
16.67	9.62	999	21.01	2.18
25	14.43	1467	30.85	2.14
0	0	1000	21.03	0
0	0	1400	29.44	0

Plots of the flow in the inlet at station 3 are shown in Figs. 12 and 13. In these figures the position of the pump wall and hub are shown by the outer and inner black circles, respectively. It was not possible to measure all the way to the hub or the wall due to light reflection off of the solid surfaces. Also, both plots show a region below and to the right of the shaft which has no data. This is the region of the flow shadowed by the hub, as explained in the *Experimental Procedure – Probes* section. The measurement grid for station 3 is shown on top of the velocity fluctuation contours of Fig. 13.

The axial velocity at station 3, Fig. 12, shows a large gradient from the top to the bottom of the rotor disk. Even though only a single component of velocity was measured at this station, it is apparent that there is swirl in the inflow. The shaft wake, seen as the region of low velocity and high turbulence above the hub in the two figures, is clearly skewed in the direction of the rotor rotation. In addition, the portion of near-wall flow which has the lowest velocity and highest turbulence is not at the top of the pump, but rather to the outboard side, which is the direction of the pump rotation. The rotor rotation is being felt upstream, most likely through the wall and shaft boundary layers.

Plots of the mean flow at station 6 are shown in Figs. 14 - 18. All plots show a swirl over most of the flow in the direction of the rotor rotation, and reversed swirl in the hub wake. In the three underway plots, the flows are nearly identical, with the 16.67 kt. case showing slightly increased velocity compared to the other two speeds. The plots of the mean flow at the two bollard conditions, Figs. 17 - 18 are also nearly identical. They differ from the underway plots in having hub wakes which are broader and which extend more to the lower outboard side.

Plots of the velocity fluctuations in the flow are shown in Figs. 19 - 23. Again, the three underway plots are nearly identical to one another, and the two bollard plots are nearly identical as well. There are

some small differences between the underway and bollard plots, though. The turbulent region behind the hub is somewhat smaller in the bollard flow, and has a more flattened shape then in the underway flow. The underway plots also show greater turbulence near the lower wall than for the bollard plots.

Integrated Flux Coefficients

The velocity fields were interpolated to the walls and integrated, as explained in the *Procedure – Data Reduction* section, to obtain the average velocity and flow rate, and the momentum and energy non-uniformity coefficients. The results of these integrations are listed in Tables 3 and 4. The flow rate at 25 kt was found both at station 3 and at station 6. The flow rate calculated at these two stations differs by 3.5%. With the accuracy of the flow rate measurement at 2.8% (see next section), two separate measurements of the flux would be expected to be within 4% of one another. The measurements then agree within the expected tolerance. Since neither measurement is preferable to the other, the best estimate of the flow rate at 25 kt is the average of the two, or $0.000283 U_\infty L^2$ per pump.

Table 3. Integrated Flux Coefficients, underway.

Station	Term	Magnitude			Multiplier
		8.3 kt.	16.7 kt.	25 kt.	
3	U_{avg}			0.765	U_∞
6		1.446	1.512	1.446	
3	Q			0.000288	$U_\infty L^2$
6		0.000278	0.000291	0.000278	
3	β_M			1.019	
6		1.012	1.011	1.011	
3	β_{Ex}			1.058	
6		1.036	1.034	1.032	
6	β_{Et}	0.010	0.009	0.010	
6	β_{Er}	0.013	0.012	0.013	
6	β_E	1.061	1.056	1.055	

Flow rate through the pumps at bollard was determined by John Hoyt of Code 5500 using two other methods. In the first of these measurements, the jet outlet was directed into drums, and the time to fill the drums was measured to calculate the flow rate. In the second of these measurements, the thrust at bollard was measured and a momentum analysis was used to calculated the flow rate. These measurements are shown along with the LDV measurements of flow rate in Fig. 24. It can be seen in this figure that the three flow rate measurements agree quite well at bollard — note that the flow rate measured with the LDV should be compared to the drum fill measurement of the starboard pump. Flow rate underway was only determined with the LDV measurements, and is 12% higher than the flow rate at bollard.

Table 4. Integrated Flux Coefficients, bollard.

Term	Magnitude		Multiplier
	1000 rpm	1400 rpm	
U_{avg}	0.616	0.613	U_{tip}
Q	1.19E-04	1.18E-04	$U_{tip}L^2$
β_M	1.008	1.009	
β_{Ex}	1.025	1.026	
β_{Et}	0.010	0.010	
β_{Er}	0.015	0.015	
β_E	1.051	1.053	

UNCERTAINTY ANALYSIS

Elemental Uncertainties

The uncertainties for the fundamental quantities measured in this experiment are listed in Table 5. Those uncertainties which are the same for all measurements are listed as bias uncertainties, and those uncertainties which vary for each measurement are listed as precision uncertainties. Uncertainties are listed as a fraction of the nominal value, unless otherwise noted.

Table 5. Elemental uncertainties.

Item	Bias	Precision	Item	Bias	Precision
U_∞	0.0001	0.0001	$\Delta x\ (U_2-U_1)$	0.000009 L	
d_f	0.003		$\Delta y\ (U_2-U_1)$	0.000009 L	
x	0.00018 L		$\Delta z\ (U_2-U_1)$	0.00002 L	
y	0.00018 L		$\Delta x\ (U_2-U_3)$	0.00002 L	
z	0.00018 L		$\Delta y\ (U_2-U_3)$	0.00002 L	
θ_3	0.08°		$\Delta z\ (U_2-U_3)$	0.00002 L	

The uncertainty in d_f is the uncertainty in the fringe spacing, or the uncertainty in the LDV probe calibration. The uncertainties in x, y, and z are the uncertainties in positioning the probe volume with respect to the model. The Δx, Δy, and Δz uncertainties are the uncertainties in positioning the three probe volumes with respect to each other, with the position of the second measured component defined for the purpose of calculation to be the measurement point. Uncertainty in the measurement of the frequency is assumed to be small relative to the uncertainty due to finite sample size, and so is ignored.

Calculated Uncertainties

The calculated uncertainties are found by combining the above component uncertainties with information on the flow conditions. The bias uncertainty arises from bias in the measured components of velocity, uncertainty in the relative component positions, and uncertainty in the component angles. For example, for the z-component of velocity, the bias uncertainty is:

$$B^2(U_z)=\left(\frac{\partial U_z}{\partial U_2}B(U_2)\right)^2+\left(\frac{\partial U_z}{\partial U_3}B(U_3)\right)^2+\left(\frac{\partial U_z}{\partial \theta_3}B(\theta_3)\right)^2+\left(\frac{\partial U_z}{\partial U_3}\frac{\partial U_3}{\partial y}B(\Delta y_{23})\right)^2$$
$$+\left(\frac{\partial U_z}{\partial U_3}\frac{\partial U_3}{\partial z}B(\Delta z_{23})\right)^2$$

No term for Δx is included in the equation since velocity gradients in the x direction are assumed to be small.

Precision, or random uncertainty arises due to measuring a fluctuating quantity with a finite number samples in the measured velocity. The precision uncertainty (95% confidence interval) is $2 \cdot q/n^{0.5}$, or for a sample size of 20000 measurements, $P(U_i) = 0.015\ q$. The resultant total uncertainty for each component of velocity, $U(U_i)$, is then:

$$U^2(U_x)=B(U_1)^2+\left(\frac{\partial U_x}{\partial y}B(\Delta y_{12})\right)^2+\left(\frac{\partial U_x}{\partial z}B(\Delta z_{12})\right)^2+0.0002q^2 \tag{8}$$

$$U^2(U_y)=B(U_1)^2+0.0002q^2 \tag{9}$$

$$U^2(U_z)=\left(\frac{B(U_2)}{\tan\theta_3}\right)^2+\left(\frac{B(U_3)}{\sin\theta_3}\right)^2+\left[\left(\frac{U_2-U_3\cos\theta_3}{\sin^2\theta_3}\right)B(\theta_3)\right]^2+\left(\frac{\partial U_z}{\partial y}B(\Delta y_{23})\right)^2$$
$$+\left(\frac{\partial U_z}{\partial z}B(\Delta z_{23})\right)^2+0.0002q^2 \tag{10}$$

Since the uncertainty of the measurements is dependant on the conditions of the flow, it is not possible to assign a single number to the velocity uncertainty. Instead, the uncertainty was calculated at all points in the flow. At almost all points, the largest source of uncertainty is the precision uncertainty. This uncertainty is the same for all three components of velocity, so the total uncertainty for the three components is similar.

The bias and total uncertainty in the axial velocity component at station 3 is shown in Figs. 25 and 26 respectively. The bias uncertainty is directly proportional to the velocity in the flow, and so is a maximum at the bottom of the pump and is a minimum in the shaft wake. The precision uncertainty is a function of the turbulence level and so is a minimum at the bottom of the pump and is a maximum in the shaft wake. For this reason the total uncertainty in Fig. 26 is nearly constant across the passage at $0.003U_\infty$.

The bias and total uncertainty in the axial velocity component at station 6 at 25 kt is shown in Figs. 27 and 28 respectively; the plots at the other speeds are nearly identical. Over most of the passage the

magnitude of the precision and bias uncertainties are similar, with the precision uncertainty generally being higher. This is particularly true behind the hub. Total uncertainty ranges from 0.005 to $0.01U_\infty$, with the average uncertainty at $0.007U_\infty$.

The total uncertainty for the horizontal and vertical velocities, U_y and U_z, are shown in Figs. 29 and 30. The uncertainties for these components are lower than for the axial component due to the lower magnitude of the velocities in these directions. The average uncertainty in U_y at station 6 is $0.0044U_\infty$ and the average uncertainty in U_z is $0.0049U_\infty$.

Uncertainty in the velocity measurements at the bollard condition is very similar to that in the underway condition. The total uncertainty in the axial velocity component at station 6 at 1400 rpm is shown in Fig. 31. The distribution is very similar to that shown in Fig. 28, with the magnitude being different due to the different normalization. The average uncertainty in U_x at station 6 in the bollard condition $0.003U_{tip}$. The uncertainty at 1000 rpm is nearly identical.

Uncertainty in the root-mean-square of the velocity fluctuations, q, is a precision uncertainty and comes from 2 terms. The first is finding the variance of the velocity using a finite sample size. For a sample size of 20,000, the uncertainty in the rms is $0.01q$. Experience has shown that a second source of uncertainty in q is the longer term fluctuations in the flow, which cause a larger uncertainty in the rms. It is estimated that the precision uncertainty from both terms is $0.03q$.

The primary source of uncertainty in the integrated flux terms is due to the regions of the flow which could not be measured. At station 3 approximately 14% of the passage could not be measured, and at station 6 approximately 12% of the passage could not be measured. It is estimated that the average velocity in this unmeasured region can only be approximated to 20% accuracy. The flow in the measured area is uncertain to approximately 0.5%. Therefore the uncertainty in the average velocity in the passage, and thus the flow rate, is 2.8%.

CONCLUSIONS

An internal, three-component LDV system was used to measure the flow ahead of the rotor and inside the nozzle of a waterjet installed in a model of the R/V Athena hull. These tests revealed the flow structure within the pump, and allowed the calculation of terms required for an analysis of the pump performance. The pump was tested at three underway speeds at the self-propulsion point and at two bollard conditions. The flow at all speeds was quite similar. Flow at the inlet to the rotor showed large gradients in the flow, with a substantial gradient from the top to the bottom of the passage due to the hull interaction, and a significant shaft wake. Both the shaft wake and the inlet boundary layer are shifted in the direction of the rotor rotation at the rotor-inlet plane. These gradients in the flow are largely mixed out

through the rotor and stator, and the large gradients across the passage are largely gone by the time the flow reaches the nozzle. At the nozzle, the main sources of the flow nonuniformities are the hub and blade wakes.

ACKNOWLEDGEMENTS

The work reported here provided S&T support to a larger program funded by the Gulf Coast Region Maritime Technology Center (GCRMTC) at the University of New Orleans and administered by Band, Lavis & Associates. At NSWCCD, John Hoyt III of code 5500 was primarily responsible for the execution of that program. He and Brian Chirozzi, Bill Dryer, Jim Hickok, and Tim Smith of Code 5500 were responsible for the fabrication, setup, and operation of the model during the LDV portion of the test. They were also invaluable in integrating the LDV system with the ship and propulsor models. Alan Becnel and Mark McCain of Band, Lavis & Associates redesigned the pump housing to allow the placement of the windows for LDV probe access into the pump. Francisco (Paco) Rodriguez of Code 3610 translated the pump design into a solid model using the stereolithography system.

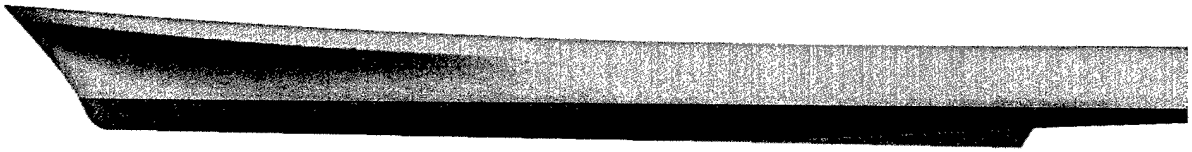

Fig. 1. Model 5600 hull, side view.

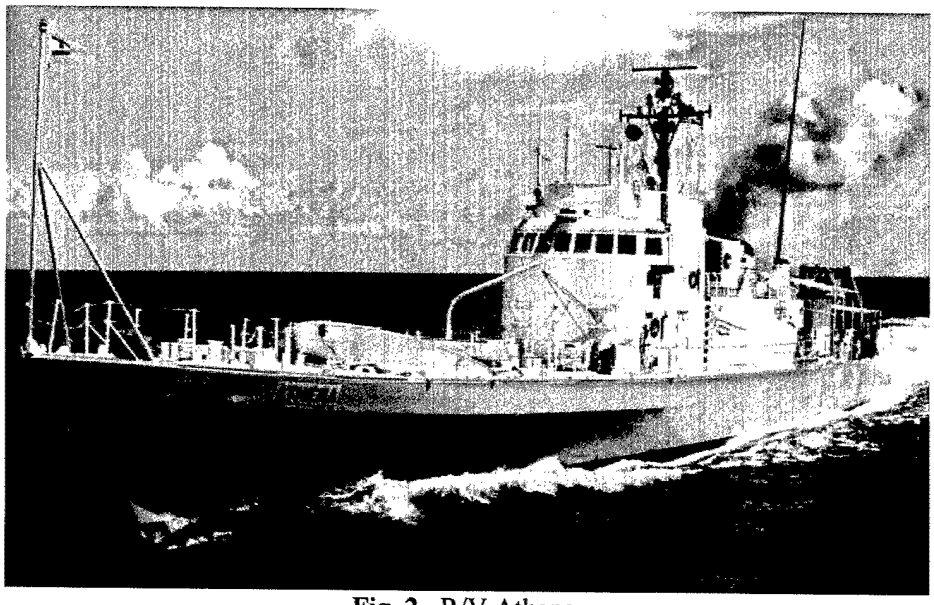

Fig. 2. R/V Athena.

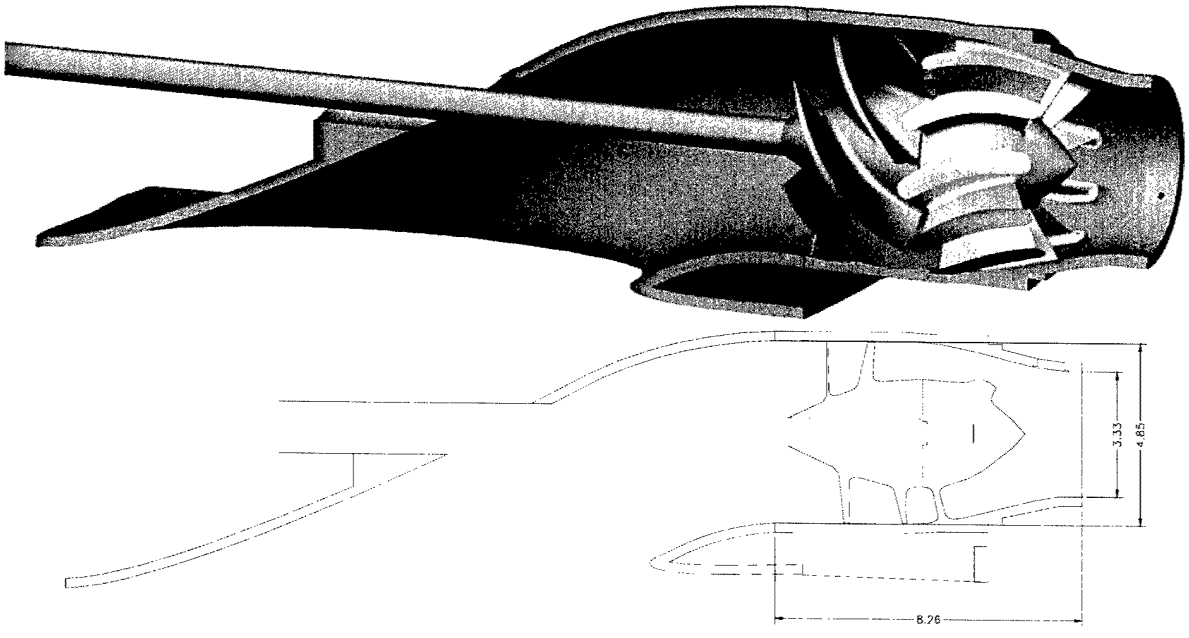

Fig. 3. Model 5600 propulsor, cutaway view.
Dimensions in inches.

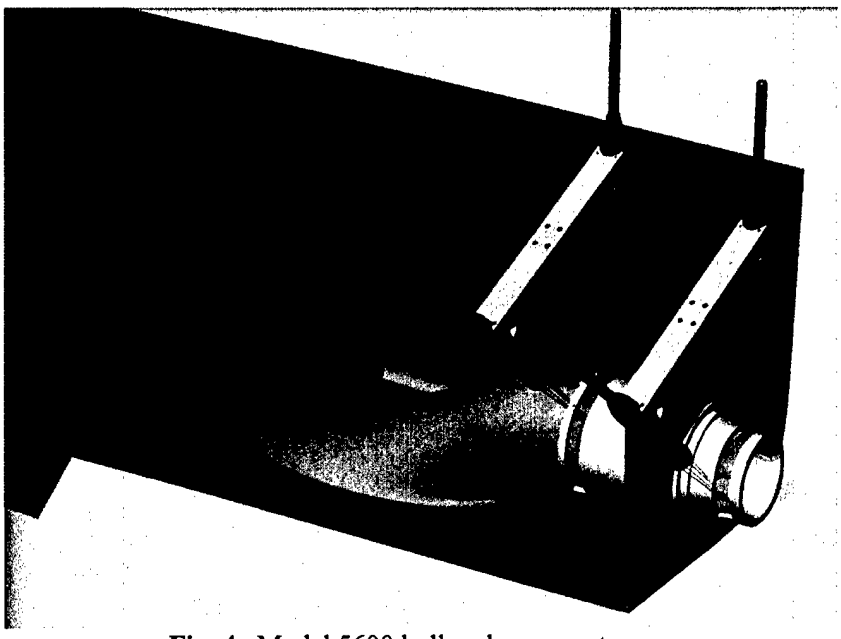

Fig. 4. Model 5600 hull and pump cutaway.
Window cutouts and LDV probes also shown.

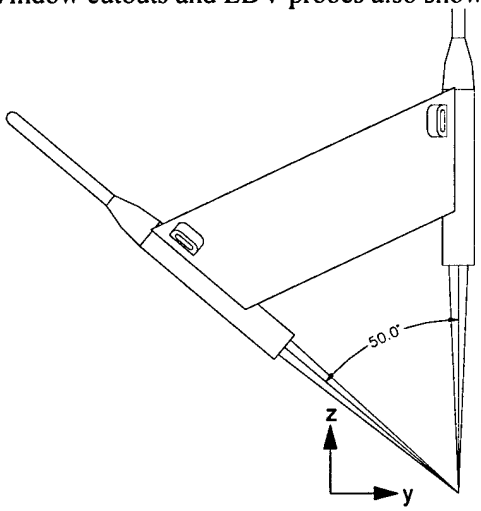

Fig. 5. Probe assembly.

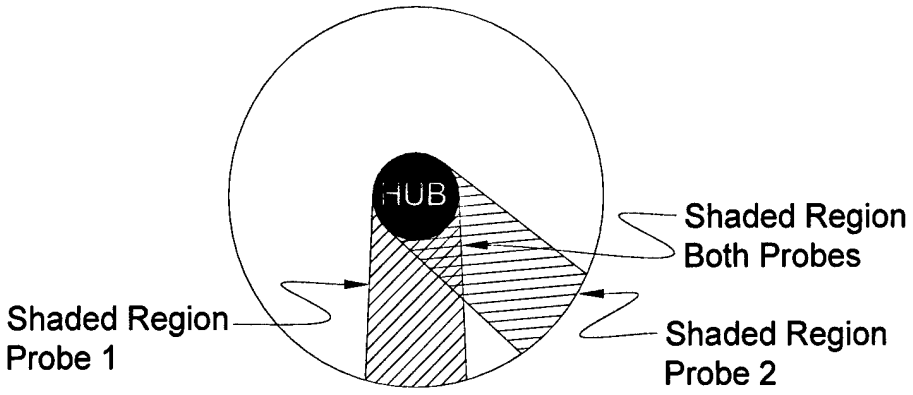

Fig. 6. Shadowed regions of flow, Station 3.

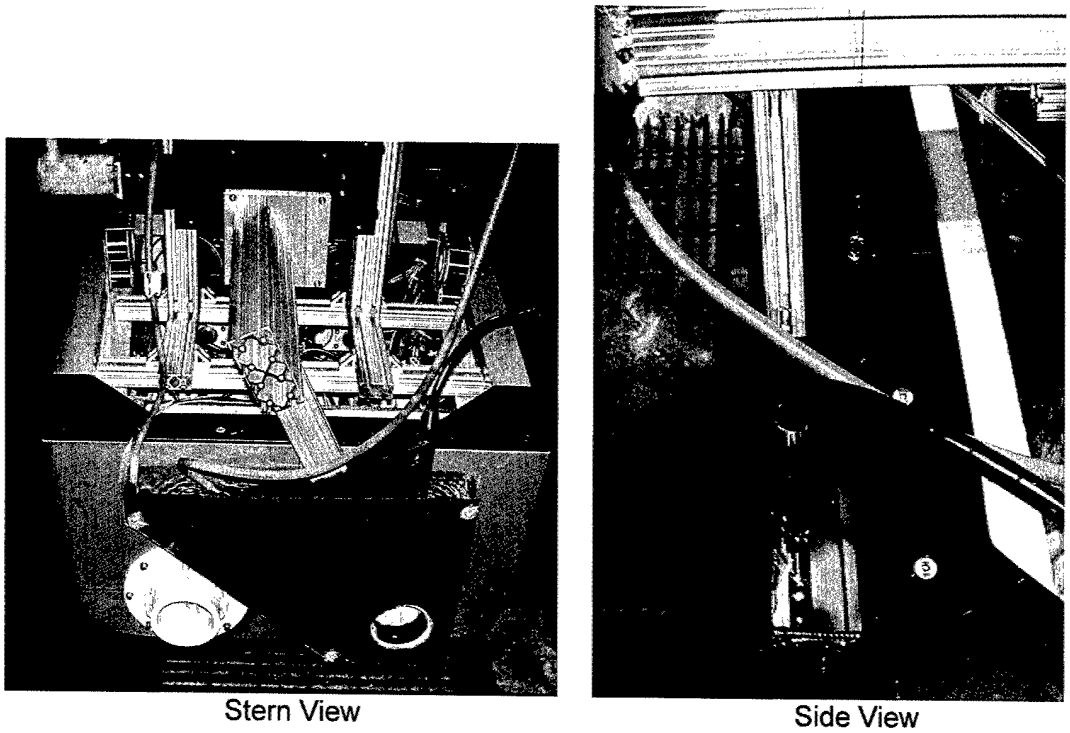

Fig. 7. Probe assembly on model at station 6.

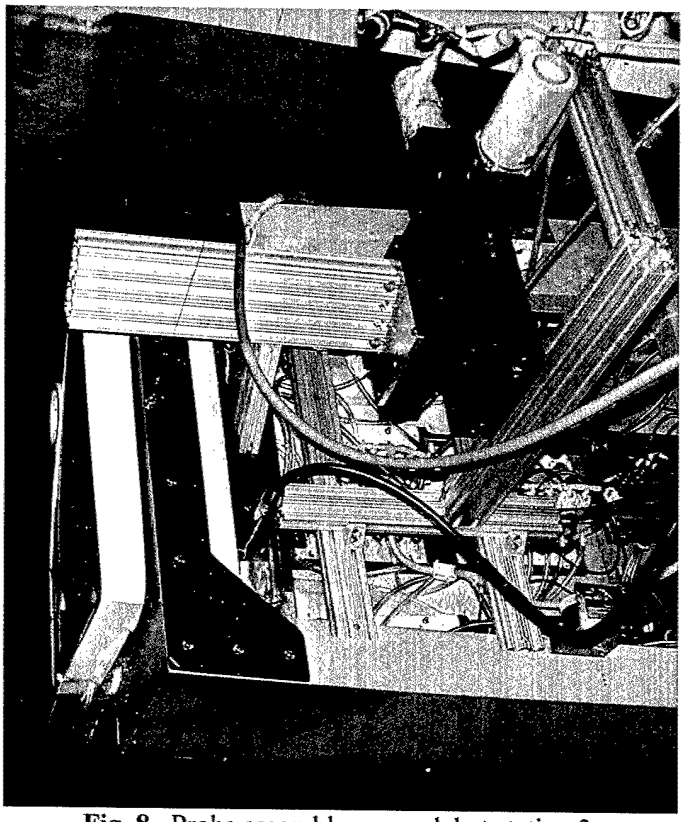

Fig. 8. Probe assembly on model at station 3.

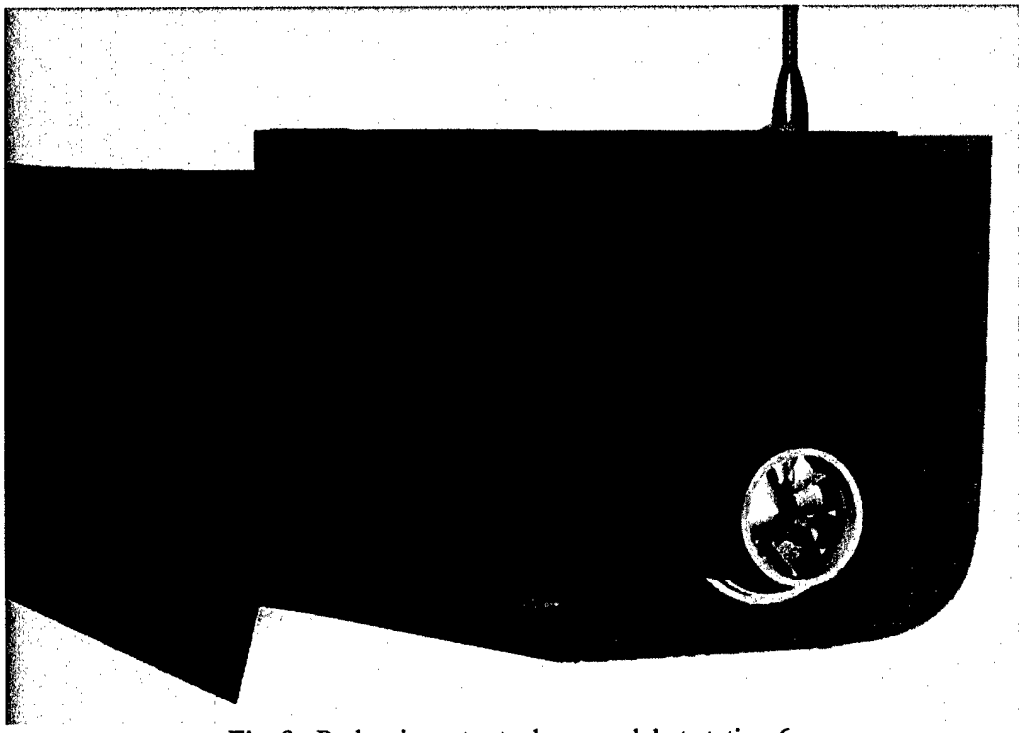

Fig. 9. Probes in water tank on model at station 6.

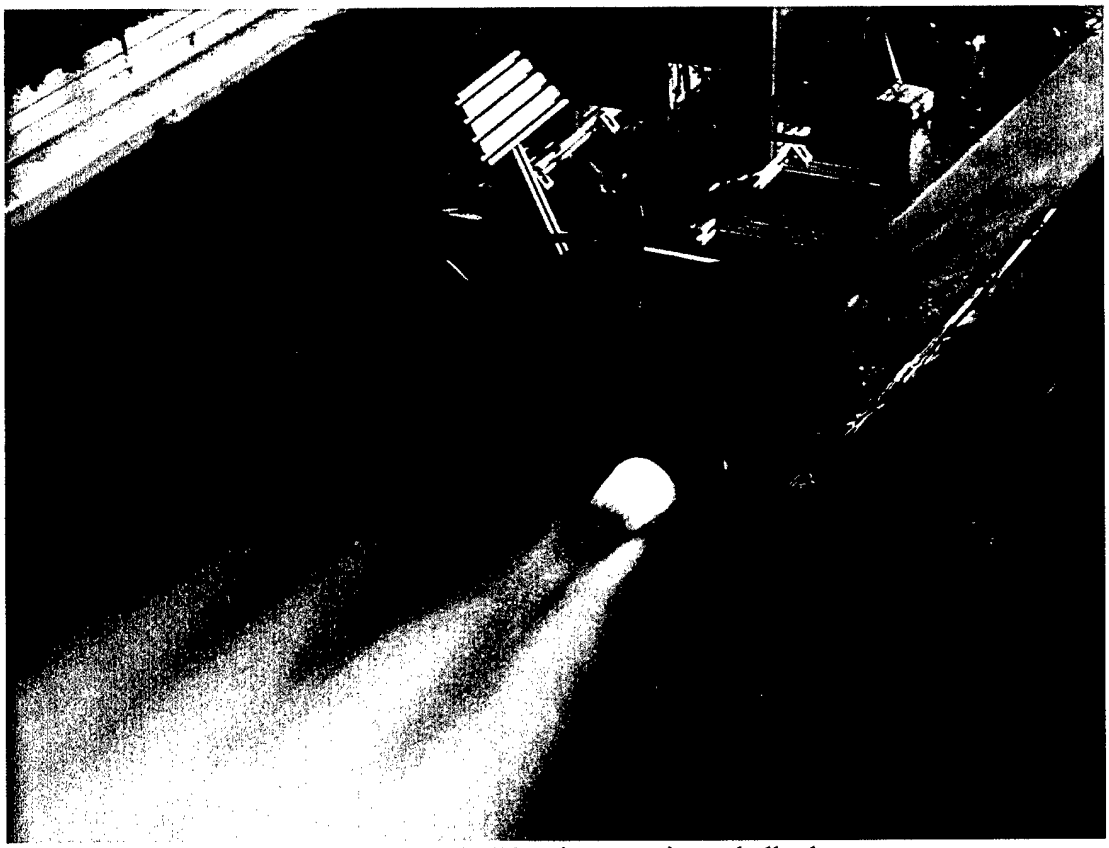

Fig. 10. Waterjet operation at bollard.

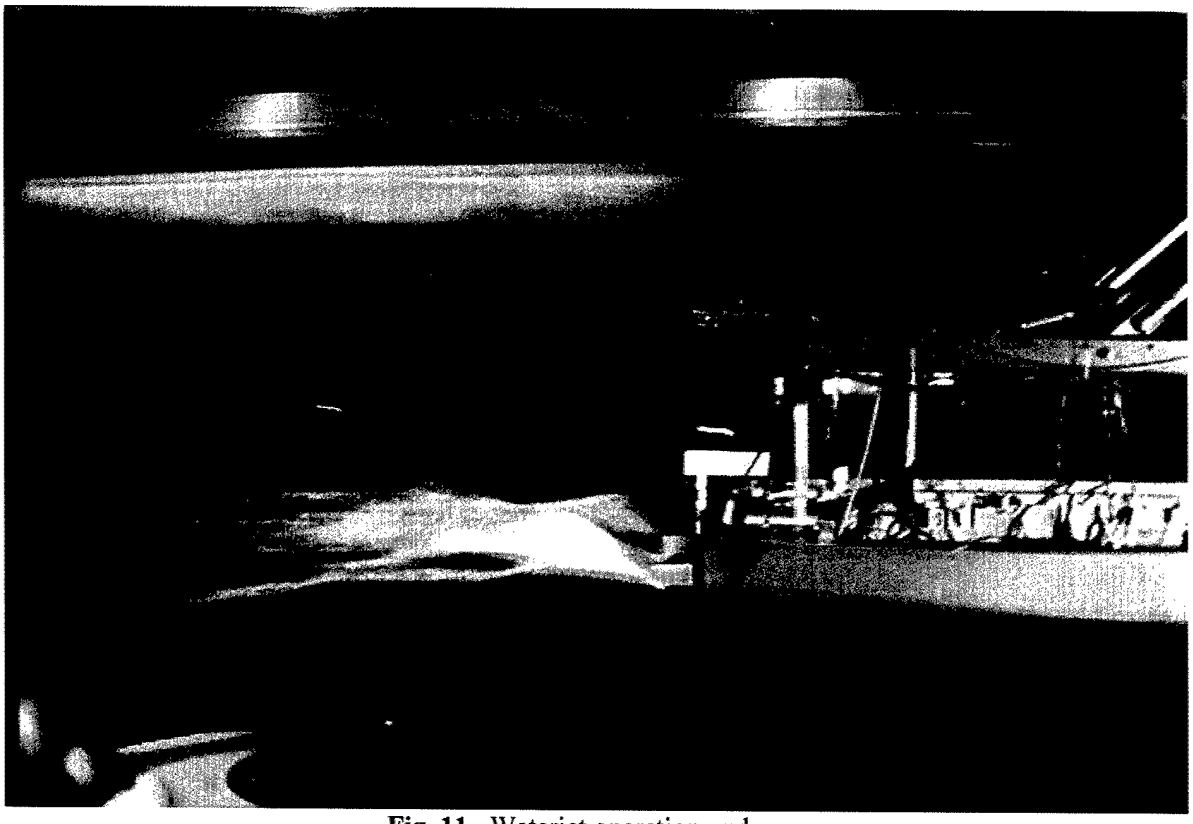

Fig. 11. Waterjet operation underway.

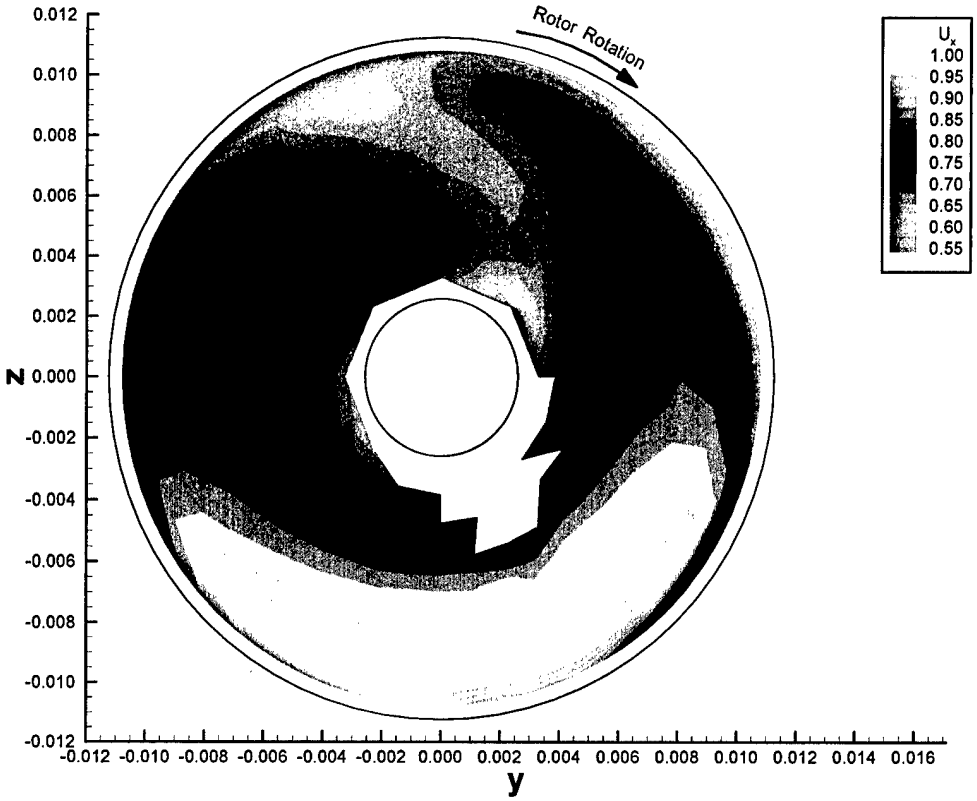

Fig. 12. Axial velocity, station 3, 25 kt. full scale.

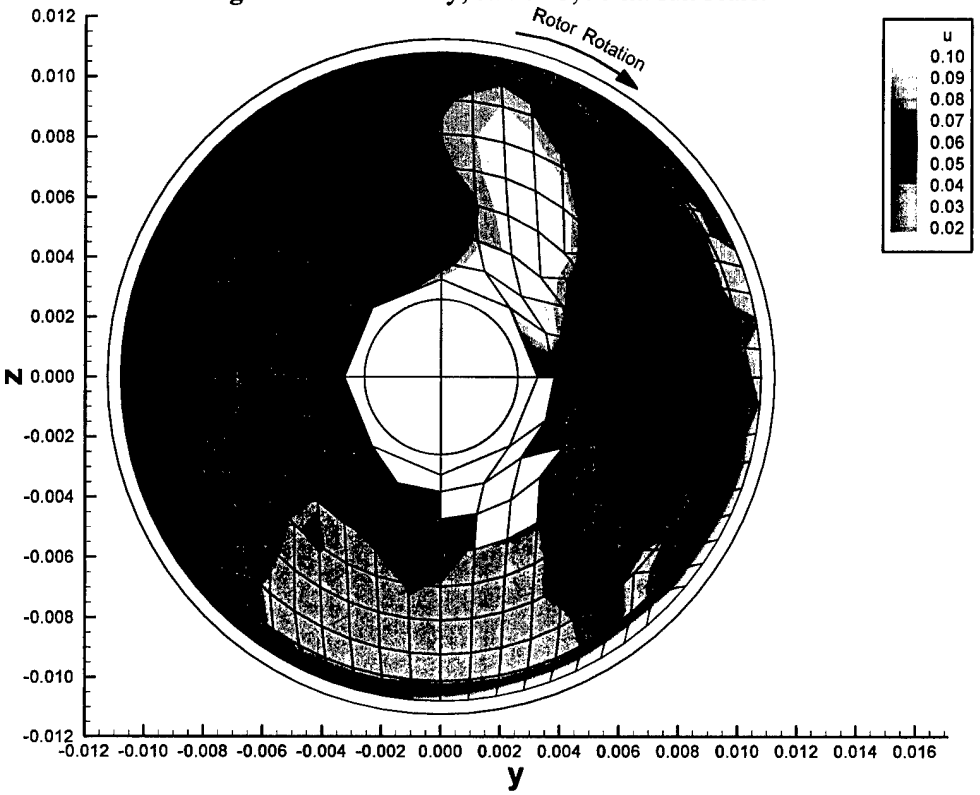

Fig. 13. Axial velocity fluctuation, station 3, 25 kt. full scale.
Black lines show measurement grid.

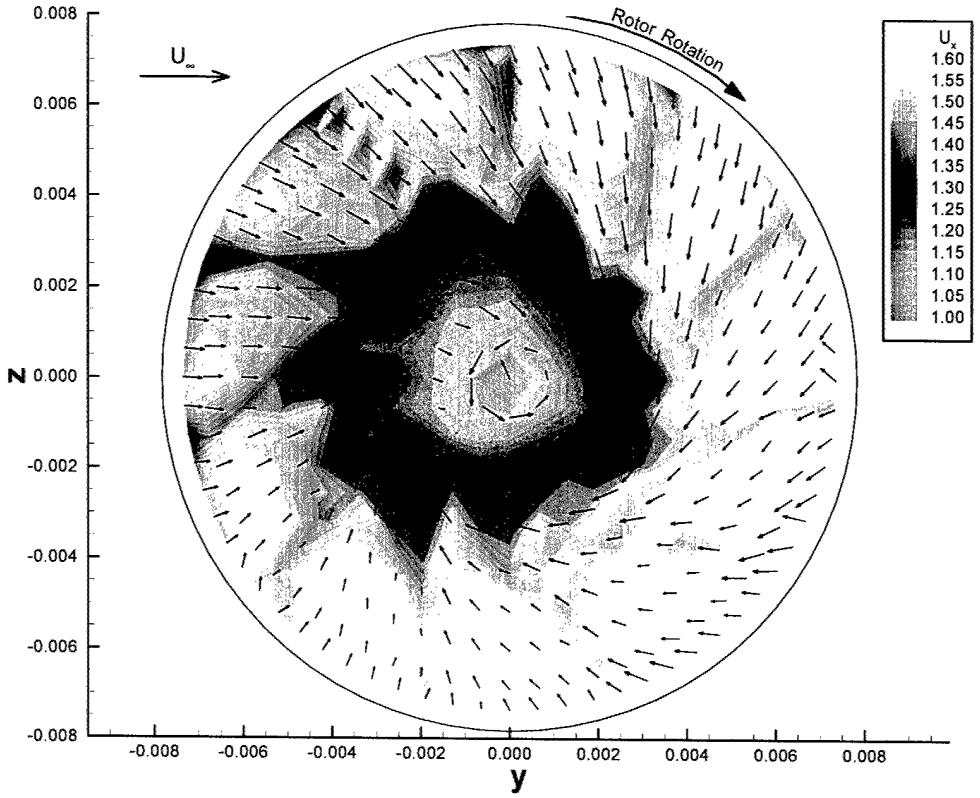

Fig. 14. Axial velocity, station 6, 25 kt. full scale.

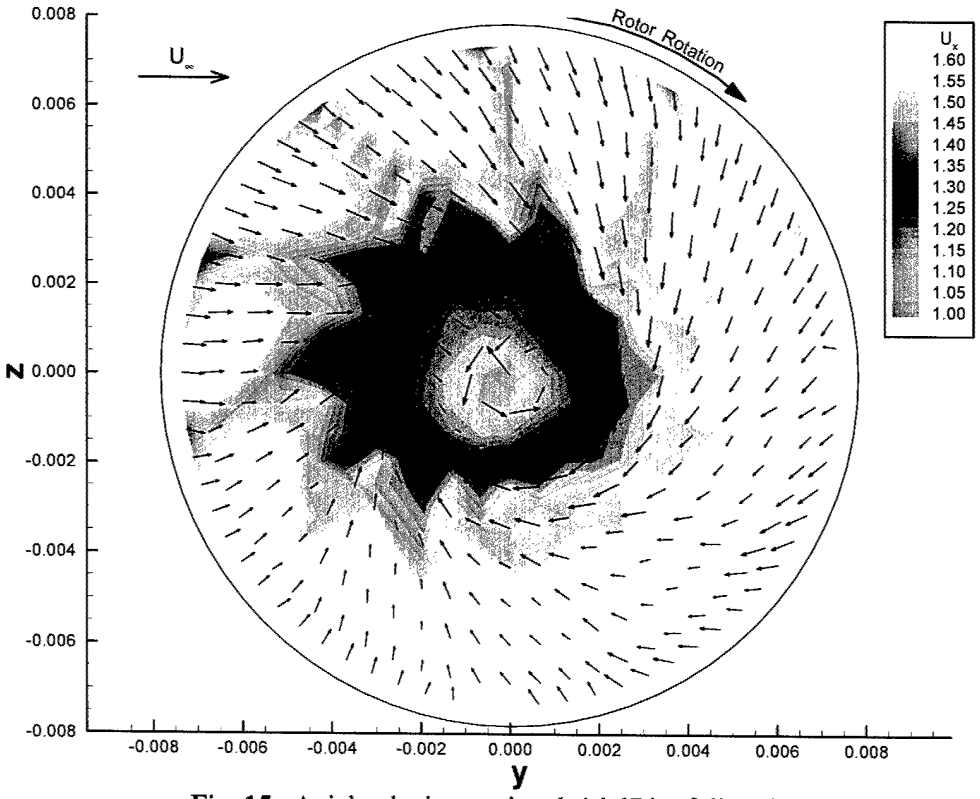

Fig. 15. Axial velocity, station 6, 16.67 kt. full scale.

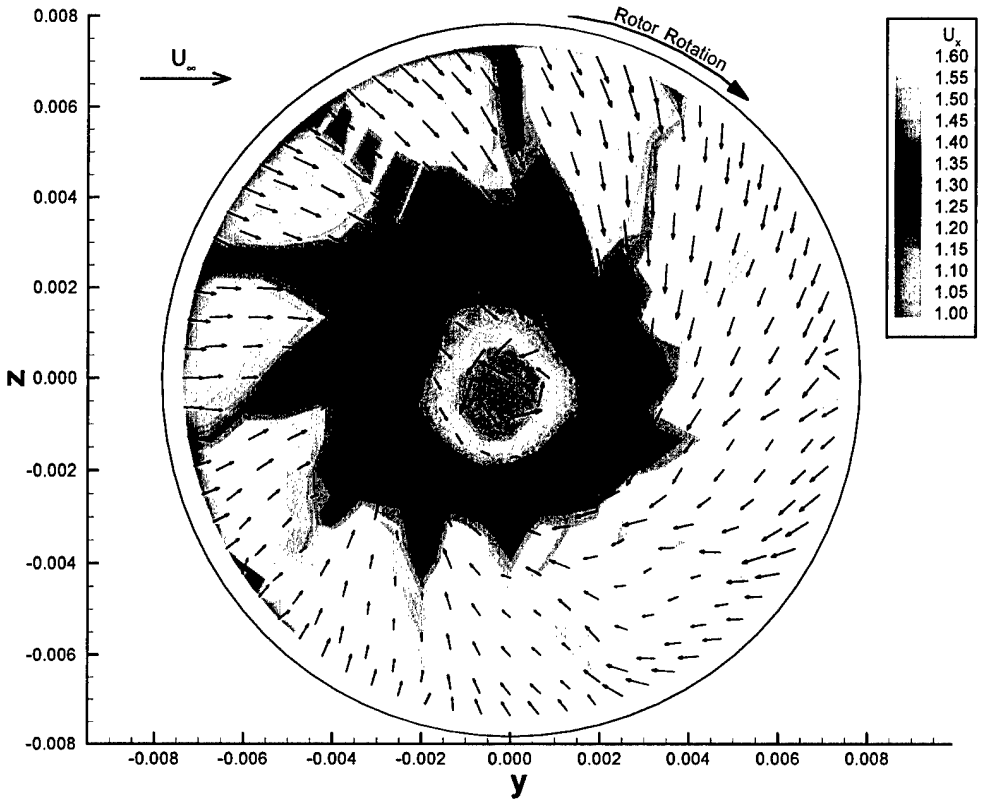

Fig. 16. Axial velocity, station 6, 8.33 kt. full scale.

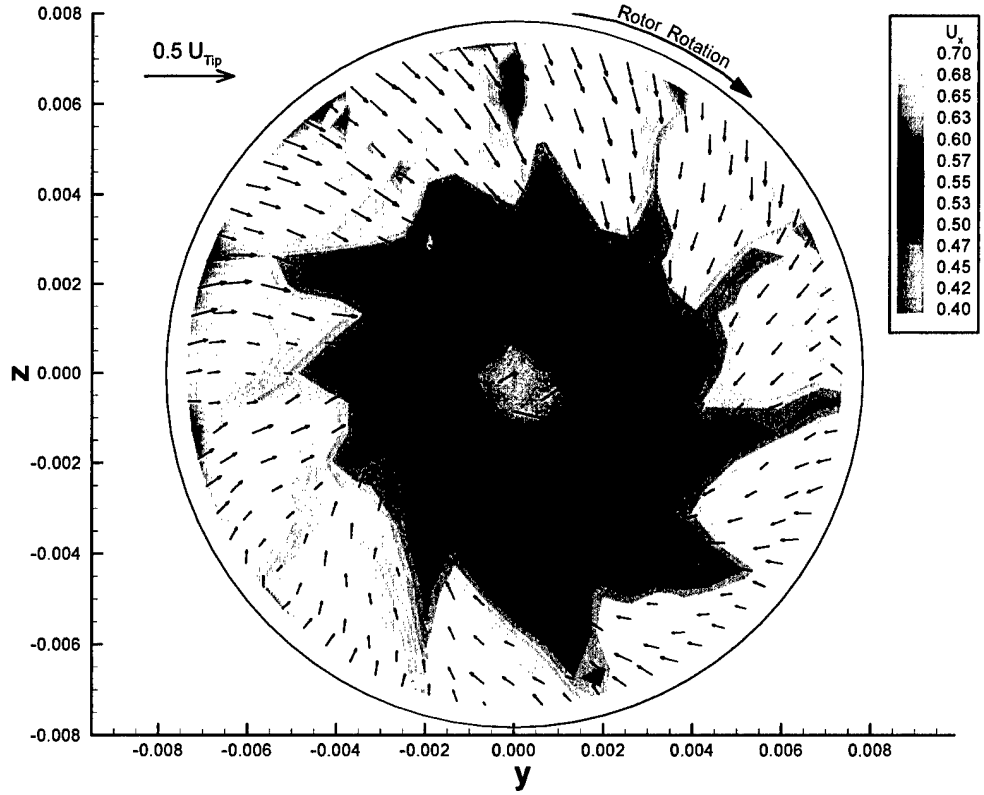

Fig. 17. Axial velocity, station 6, 1400 rpm bollard.

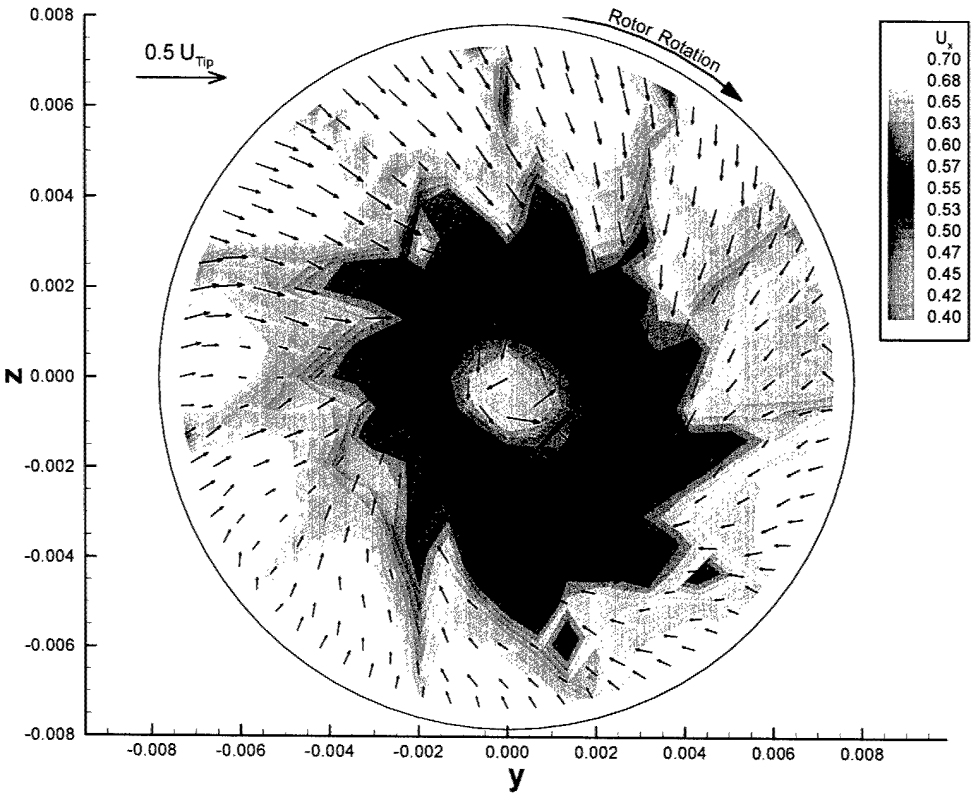

Fig. 18. Axial velocity, station 6, 1000 rpm bollard.

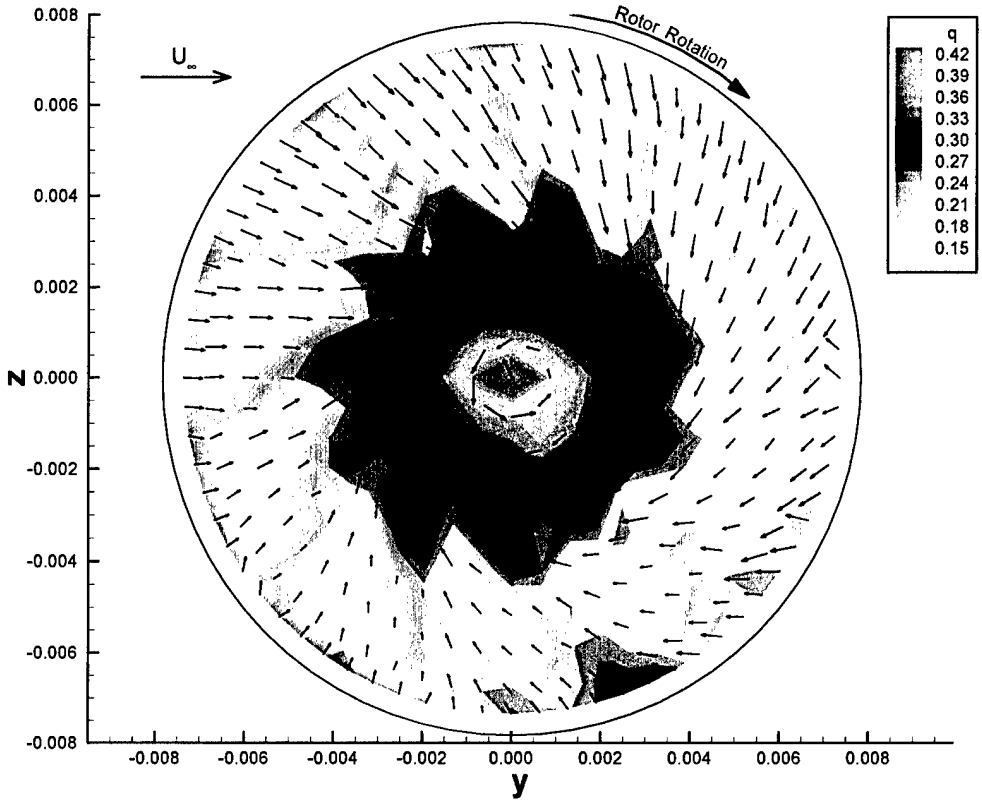

Fig. 19. Velocity fluctuations, station 6, 25 kt. full scale.

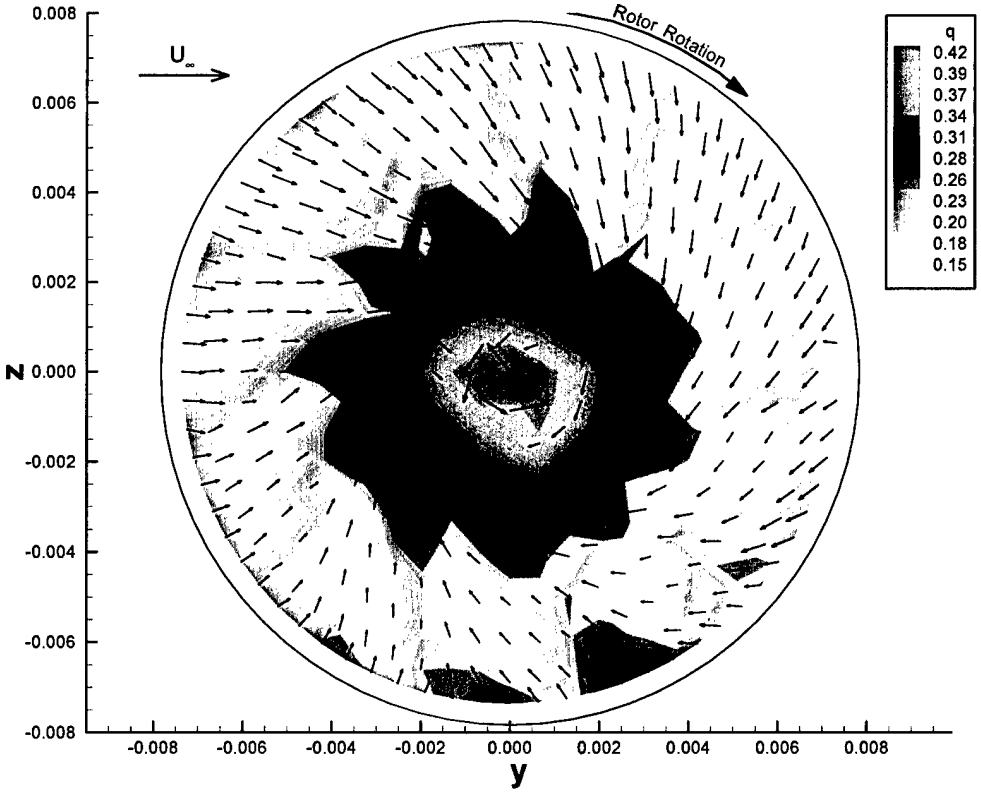

Fig. 20. Velocity fluctuations, station 6, 16.67 kt. full scale.

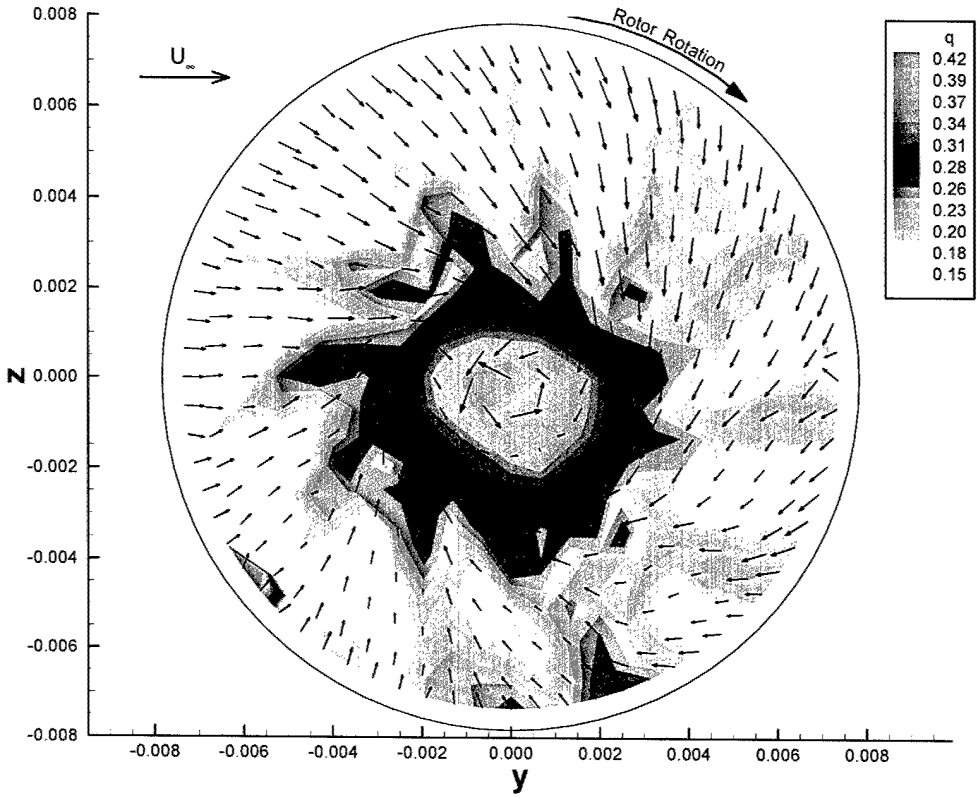

Fig. 21. Velocity fluctuations, station 6, 8.33 kt. full scale.

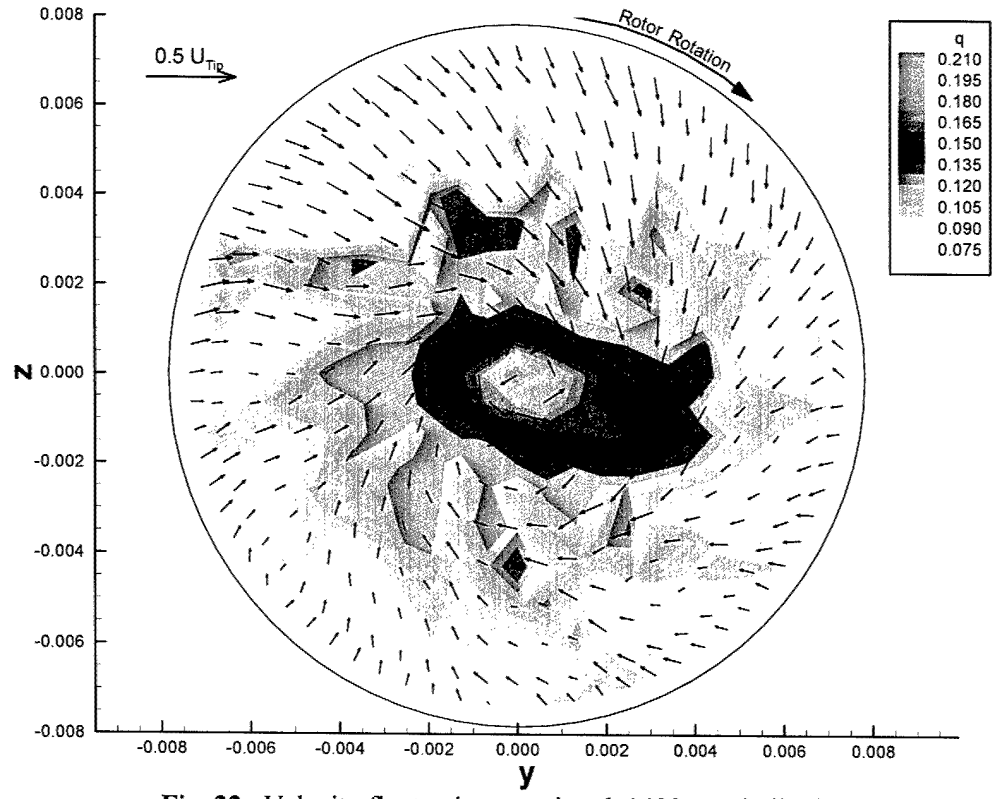

Fig. 22. Velocity fluctuations, station 6, 1400 rpm bollard.

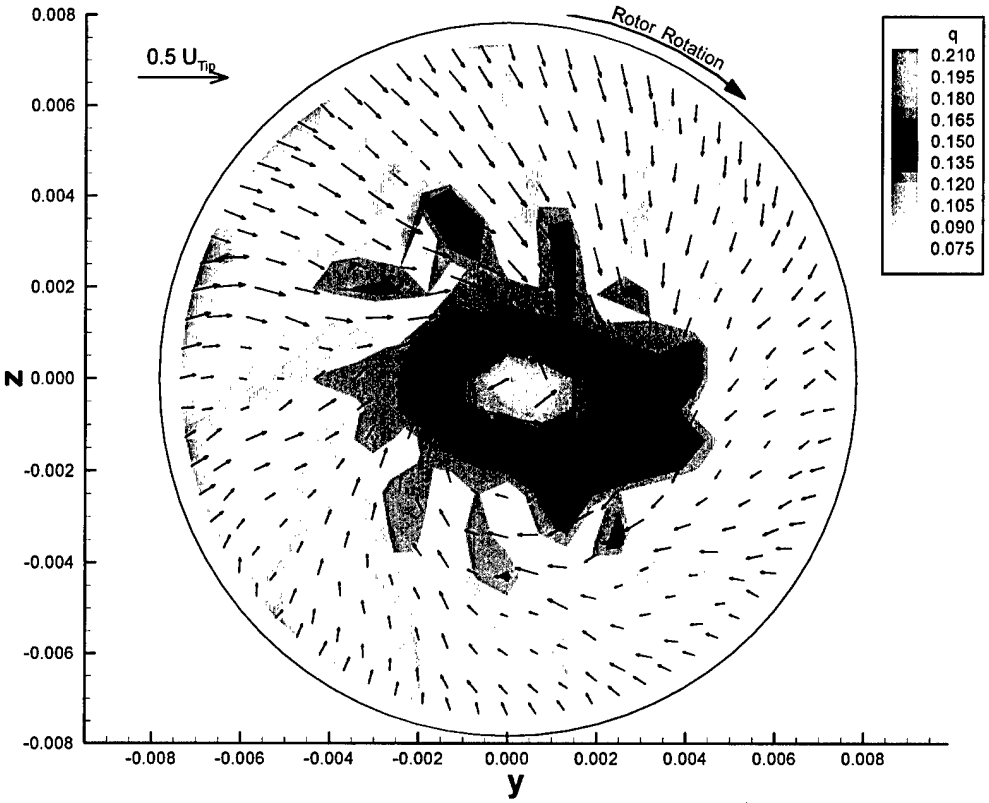

Fig. 23. Velocity fluctuations, station 6, 1000 rpm bollard.

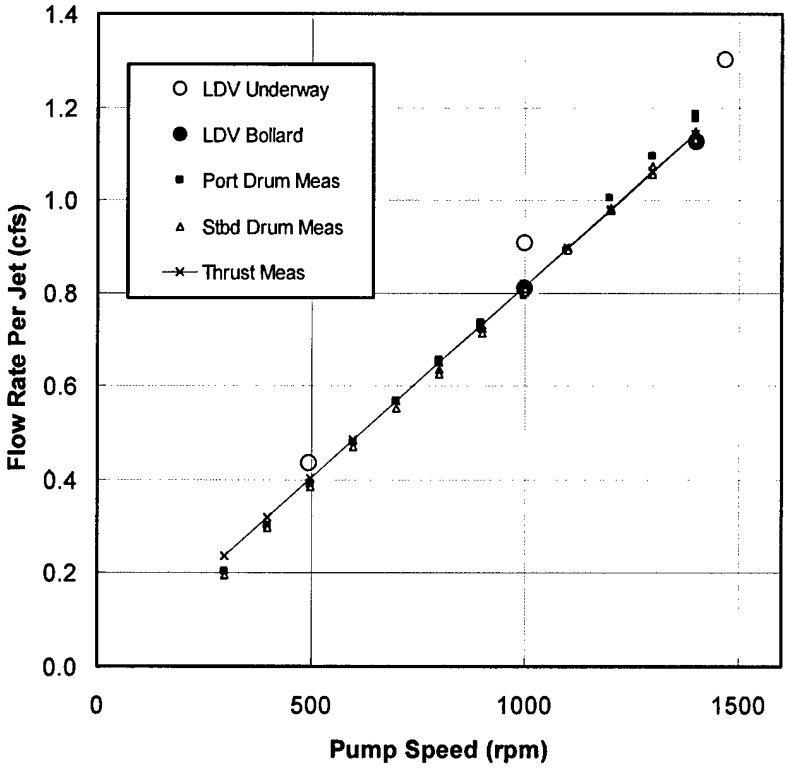

Fig. 24. Measured waterjet flow rate.

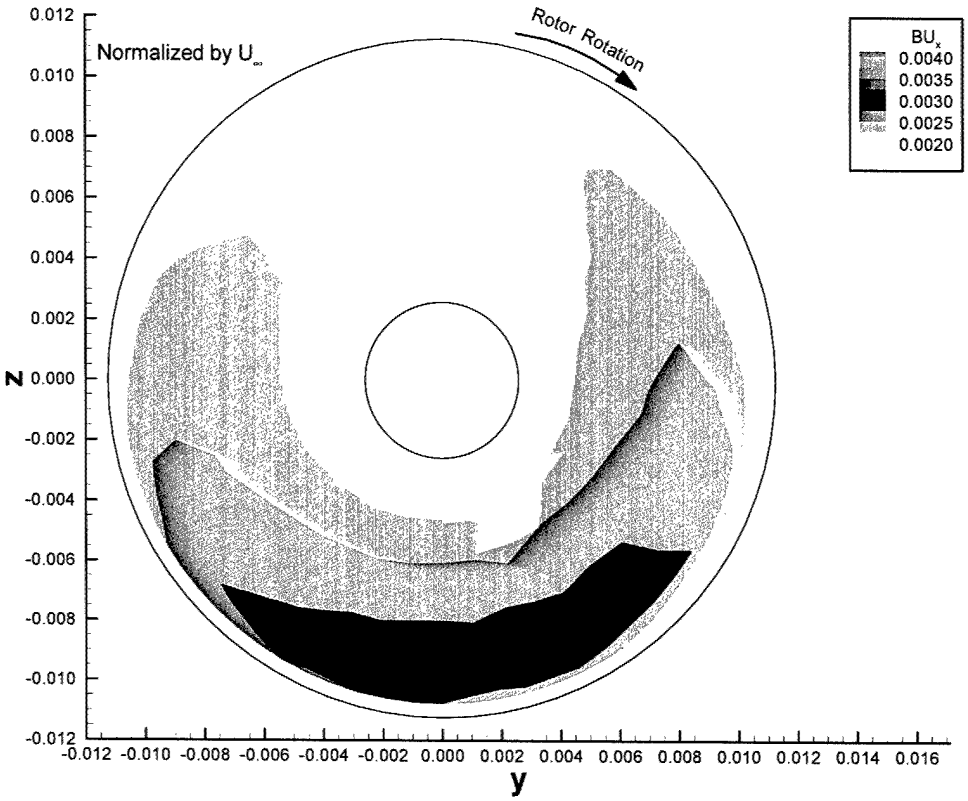

Fig. 25. Bias uncertainty in axial velocity, station 3, 25 kt full scale.

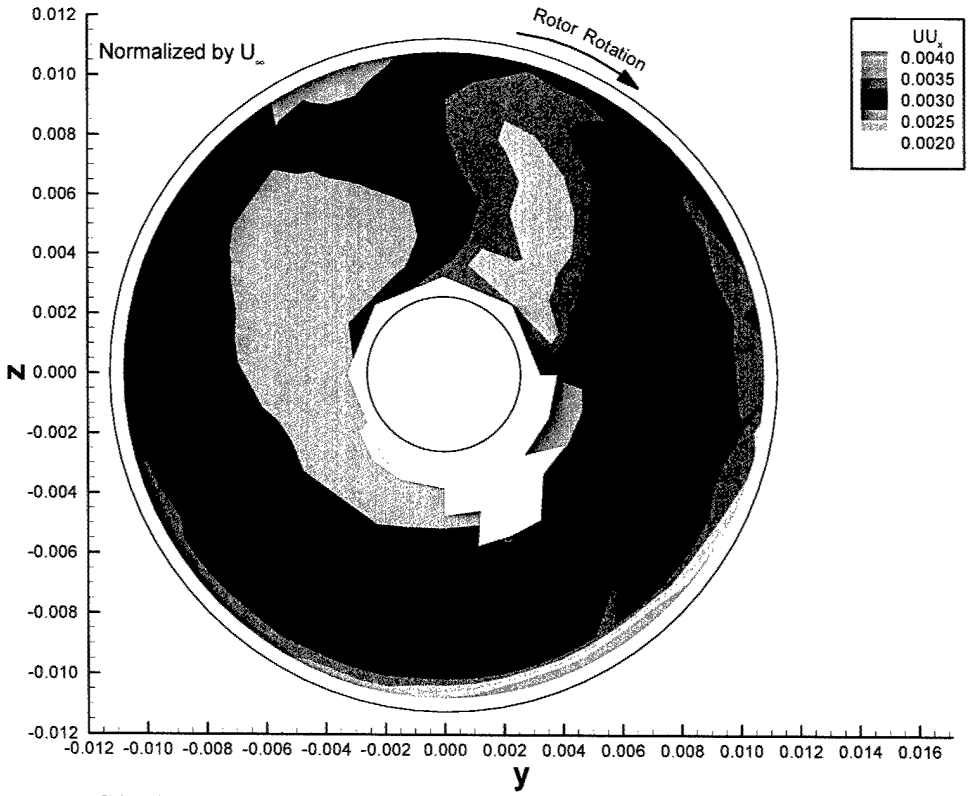

Fig. 26. Total uncertainty in axial velocity, station 3, 25 kt full scale.

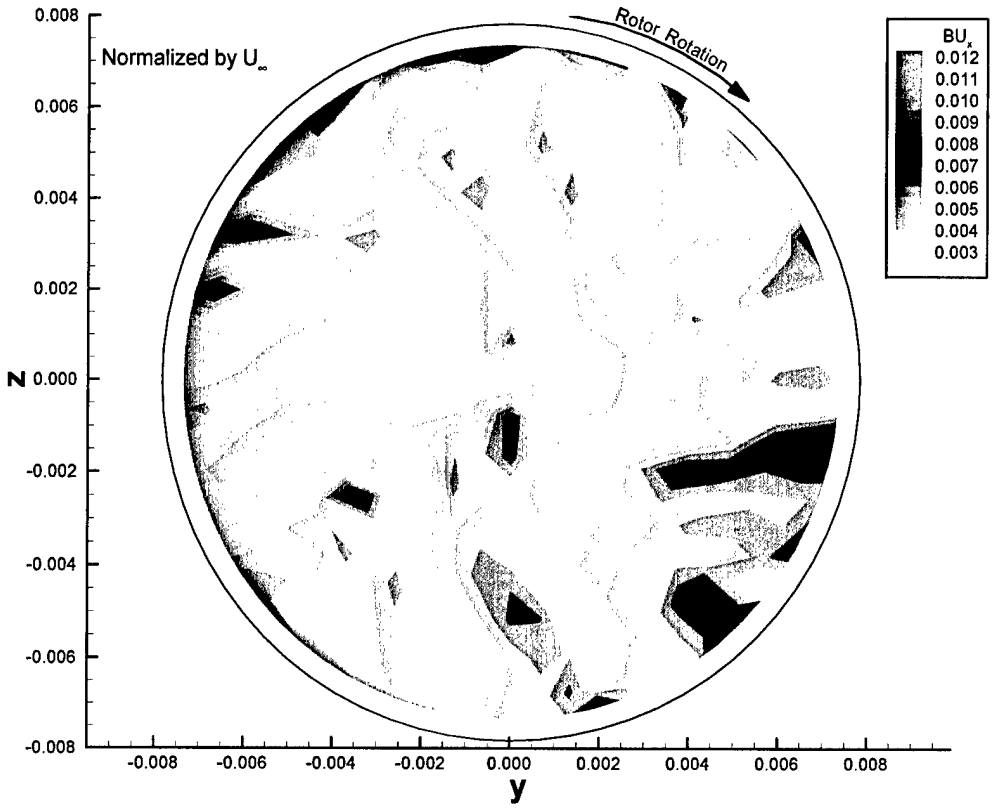

Fig. 27. Bias uncertainty in axial velocity, station 6, 25 kt full scale.

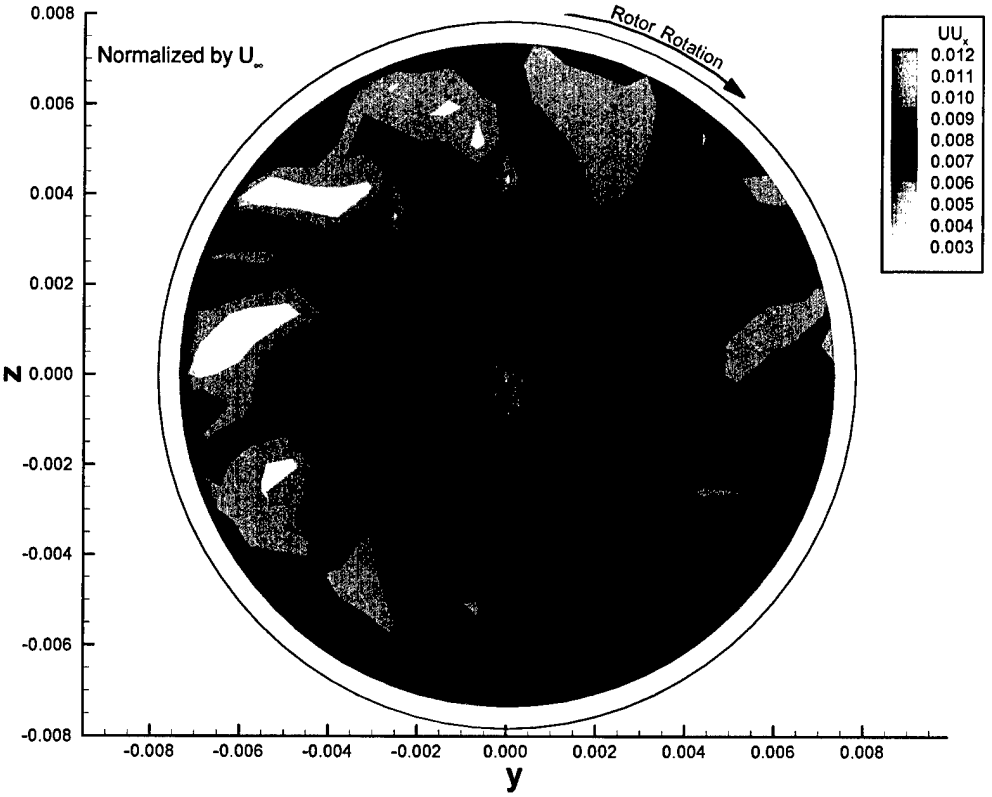

Fig. 28. Total uncertainty in axial velocity, station 6, 25 kt full scale.

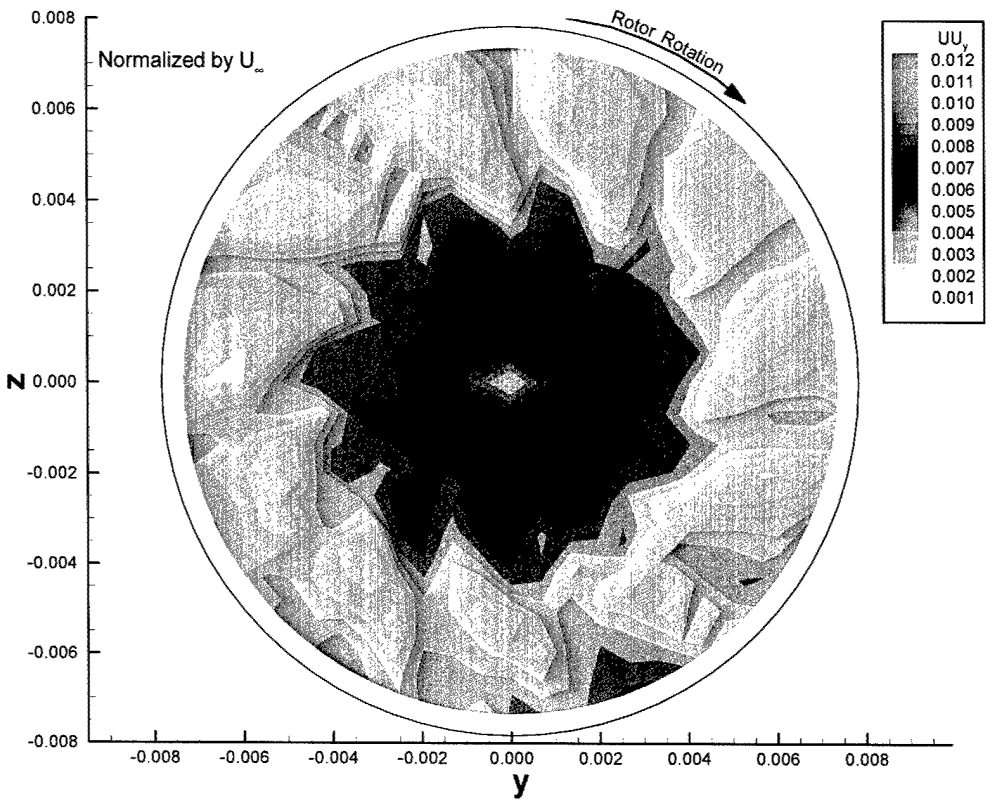

Fig. 29. Total uncertainty in horizontal velocity, station 6, 25 kt full scale.

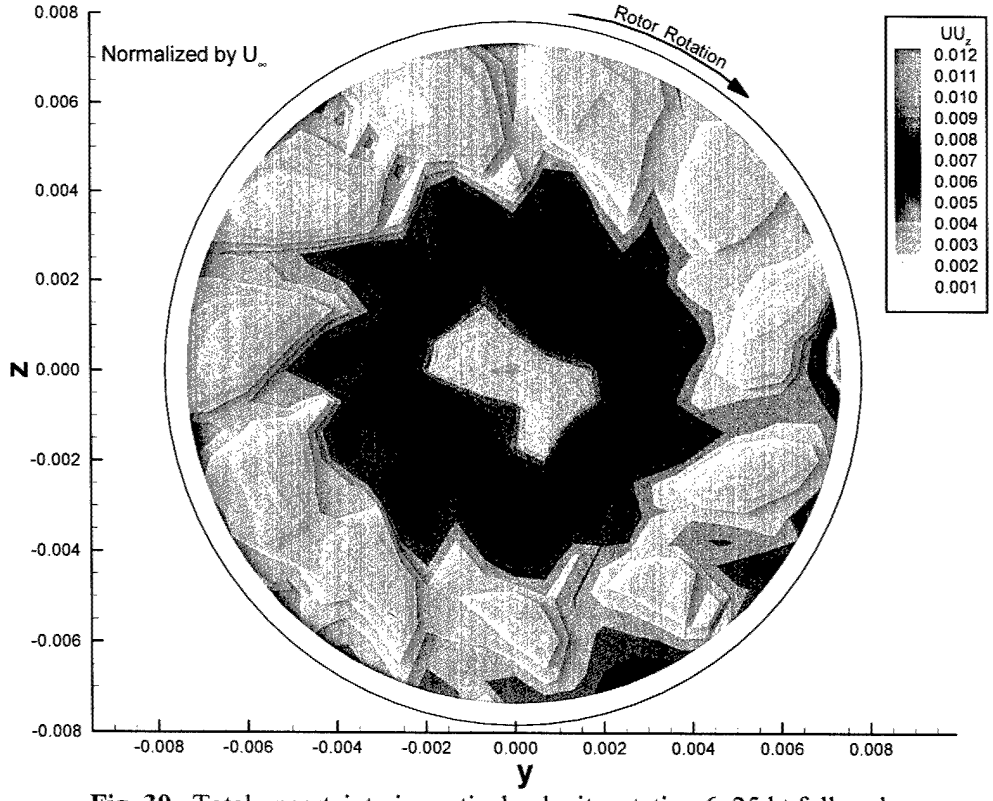

Fig. 30. Total uncertainty in vertical velocity, station 6, 25 kt full scale.

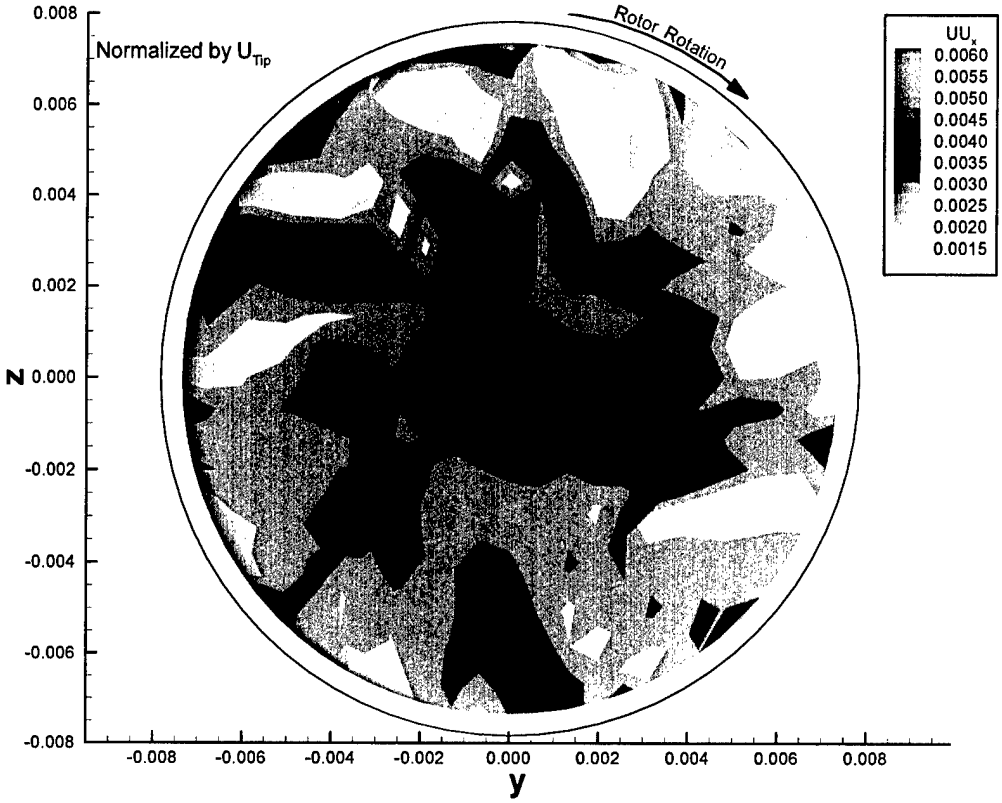

Fig. 31. Total uncertainty in axial velocity, station 6, 1400 rpm bollard.

INITIAL DISTRIBUTION

Organization	Name	Copies
ONR		
361	J. Carney	1
333	K. H. Kim	1
333	S. Schreppler	1
33X	J. Webster	1
NAVSEA		
05H	C. Crockett	1
	J. Schumann	1
Band, Lavis & Associates		
	A. Becnel	1
	J. Purnell	1
	D. Lavis	1
General Dynamics		
	M. Widner	1
	T. Faria	1
University of New Orleans GCRMTC		
	J. Crisp	1
	D. Gereighty	1
	J. Smith	1
DRPM AAAV		
	S. Chun	1
	W. Zeitfuss	1
DTIC		2

CENTER DISTRIBUTION

Code	Name	Copies
0110	J. Corrado	1
	J. Barkyoumb	1
5060	D. Walden	2
5080	Brown	1
	Cox	1
5200	Day	1
	G. Karafiath	1
5400	C. Chesnakas	4
	S. Jessup	1
	T. Michael	1
	J. Scherer	1
	M. Wilson	1
	Library	1
5500	T. Applebee	1
	J. Hickock	1
	J. Hoyt	1
	T. Smith	1
	D. Woolaver	1